

Spectral multiplexing of telecom emitters with stable transition frequency

Alexander Ulanowski, Benjamin Merkel, and Andreas Reiserer*

*Quantum Networks Group, Max-Planck-Institut für Quantenoptik,
Hans-Kopfermann-Strasse 1, D-85748 Garching, Germany and*

*Munich Center for Quantum Science and Technology (MCQST), Ludwig-Maximilians-Universität München,
Fakultät für Physik, Schellingstr. 4, D-80799 München, Germany*

In a future quantum internet [1], coherent emitters [2–4] — ideally at telecommunication wavelength [5] — will exchange quantum states over global distances using optical fibers. Frequency-domain multiplexing of several [6–11] or many [12] such emitters in a single device, together with single-emitter control [13], can then facilitate entanglement [14] and local quantum information processing. This is a prerequisite for distributed quantum computing [15, 16] and enhanced communication rates via quantum repeaters [17]. So far, however, the proximity of interfaces in nanophotonic resonators has prevented such applications as it leads to spectral instability of the embedded emitters [18]. Here we demonstrate that this limitation can be overcome by embedding 19 μm thin crystalline membranes into tunable Fabry-Perot resonators with a quality factor of $Q = 10^7$. We observe and coherently control around 100 individual emitters with exceptional spectral stability of $< 0.2 \text{ MHz}$ and an optical coherence time of $0.11(1) \text{ ms}$. Our findings enable frequency-multiplexed quantum network-nodes operating at a telecommunication wavelength.

INTRODUCTION

Quantum networks can solve tasks and allow their users to interact in ways that are not possible using present-day technology [1]. Pioneering experiments have used atoms trapped in vacuum [2, 3], quantum dots [19], and color centers in diamond [4]. To access the full potential of quantum networks, these prototypes need to be scaled to longer distances and larger qubit numbers. To this end, one needs to overcome the inefficiency and imperfections of photon transmission over large distances, which can be achieved by the techniques introduced in the seminal quantum repeater proposal [17].

Implementing this and related protocols for distributed quantum computing [15, 16] requires, first, an efficient interface between the emitters and photons propagating in a single optical mode, which is feasible with suited optical resonators [3, 5–14, 19]. Second, the photons need to be emitted in [12] or converted to [20] the telecommunication frequency regime, where loss in optical fibers is minimal. Third, one needs to operate and control multiple qubits per quantum network node, e.g. by using nuclear spin registers [21] or spectral multiplexing [13, 14]. Finally, these qubits have to maintain their optical coherence during the time required to generate a photon, and their ground-state coherence until entanglement with a remote node is reliably established. Combining these four properties in a single experimental platform is an outstanding challenge.

To realize such system, we study individual erbium dopants. Among all investigated photon emitters that host long-lived qubits [22], erbium is the only one that exhibits an optical transition in the minimal-loss band of fiber-optical telecommunication, around 1536 nm. In dopant ensembles, lifetime-limited optical coherence has been achieved on this transition [5], and second-long

ground-state coherence has been observed at high magnetic fields [23]. In addition, single erbium dopants have been resolved [12] in a nanophotonic resonator, and up to four dopants have been controlled simultaneously [13]. However, in these experiments the proximity of interfaces [18] has caused fast dephasing and broadened the emission linewidth to $\sim 10 \text{ MHz}$. This has hampered the optical control of a larger number of qubits as well as the optical entanglement of erbium dopants. In this work, we overcome this limitation by avoiding the proximity of interfaces using an Yttrium-Orthosilicate (YSO) membrane in a Fabry-Perot resonator of high finesse [5], as shown in Fig. 1a.

SINGLE DOPANT SPECTROSCOPY

In YSO, the Kramers' dopant erbium [22] substitutes yttrium in two crystallographic sites. Our study is performed using site 1 that has a transition wavelength of 1536.5 nm. The relevant levels are shown in Fig. 1b. We use a nominally undoped YSO membrane of 19(1) μm thickness that contains $< 1 \text{ ppm}$ trace impurities of erbium. Thus, at the center of the 414(7) MHz full-width-at-half-maximum (FWM) Lorentzian inhomogeneous linewidth [5], the concentration of erbium is too high to resolve individual dopants. We therefore operate at several GHz detuning, i.e. at a frequency where only few erbium dopants are resonant.

The samples are cooled to $< 2 \text{ K}$ in a closed-cycle cryocooler. We apply an external magnetic field along the b axis of the crystal, such that the magnetically inequivalent classes are degenerate. The field strength is set to 2.0 or 6.8 T in order to tune the erbium transition frequency and ensure that only the lowest crystal field level Z_1 is occupied and both the erbium spin and most para-

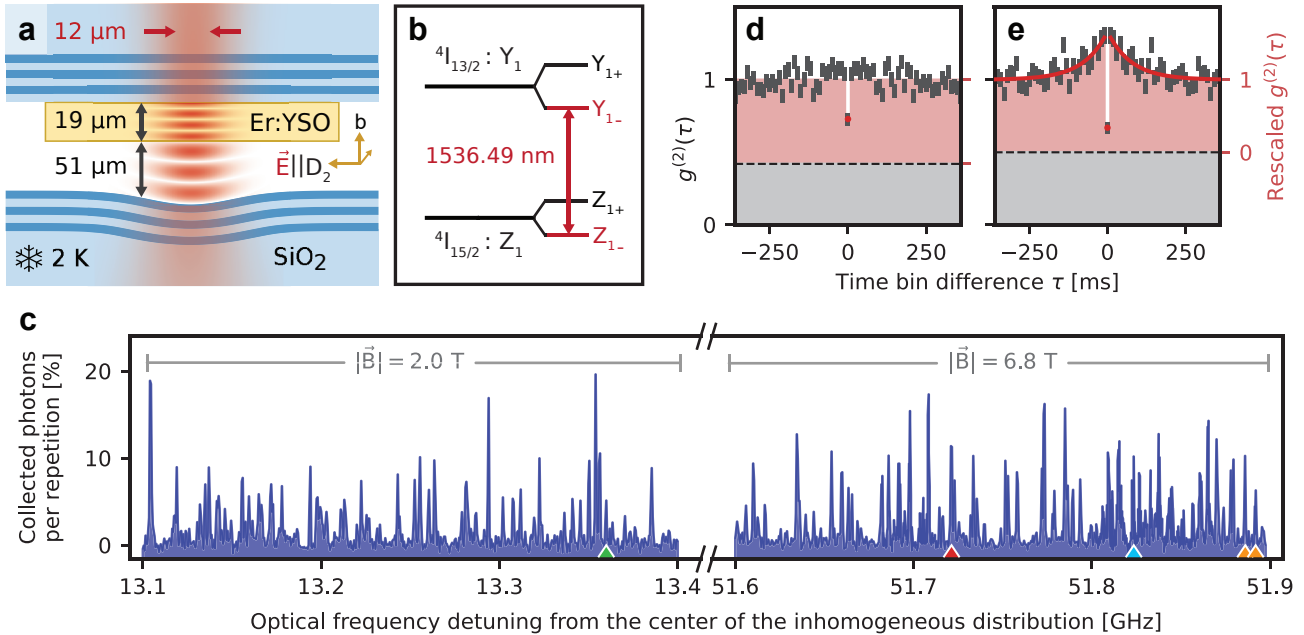


FIG. 1. **Cavity-enhanced resonance fluorescence spectroscopy.** a) Fabry-Perot cavity (not to scale). A resonator with small mode volume is formed by a flat and a concave glass mirror (blue) with deposited Bragg reflectors (dark blue), confining a stable optical mode (red). Erbium dopants are integrated in a thin, atomically flat crystalline membrane (yellow). b) Energy level scheme. The studied transition (red) is between the lowest spin and crystal-field levels of the $15/2$ and $13/2$ manifolds of erbium in YSO. c) Fluorescence spectrum. The resonator is optically excited with chirped laser pulses of 0.5 MHz bandwidth and the fluorescence is measured as a function of the detuning of the pulse center frequency from the center of the inhomogeneous distribution. Over a large frequency range, individual emitters lead to distinct narrow peaks in the spectrum, whose amplitude reflects the strength of the emitter-cavity coupling. d) and e) Photon autocorrelation function $g^{(2)}(\tau)$ measured on a randomly-chosen peak (red triangle in c); raw data (grey) and rescaled data (red) after subtracting the detector dark count contribution (dashed line). d) For fixed-frequency Gaussian excitation pulses with 0.55 MHz (FWHM) bandwidth, a rescaled $g^{(2)}(0) < 0.5$ indicates that a peak in the spectrum originates from a single emitter. e) When the excitation bandwidth is reduced to 0.28 MHz, the smaller contribution of weakly-coupled dopants gives a reduced coincidence probability at zero delay, approaching the dark count level (dashed). The temporal decay of the bunching observed for short time differences is used to determine the timescale of spectral diffusion, 80(20) ms (red exponential fit curve).

magnetic impurities are frozen to the ground state. This reduces magnetic noise from electronic spin flips.

To enhance the emission via the Purcell effect, we use a plano-concave Fabry-Perot resonator whose length can be tuned and stabilized to ± 1 pm using a piezo tube. To this end, we irradiate a laser at 1593 nm, which is far detuned from the erbium transition but resonant with another longitudinal cavity mode. The stabilization laser also leads to a slight (< 1 K) temperature increase of the crystal with respect to the cryostat temperature.

The radius of curvature of the concave mirror, c.f. Fig. 1a, is 155(3) μ m. The mirror transmissions are 22(8) ppm (for the flat outcoupling mirror with the bonded crystal) and 20(7) ppm (for the concave mirror), which is comparable to the absorption and scattering losses, 27(14) ppm. This leads to a finesse of $9.0(7) \cdot 10^4$ and a linewidth of 13(1) MHz. From the independently measured mirror parameters we expect a Purcell enhancement of $P_{\text{TL}} = 362(26)$ for a two-level system at the maximum of the cavity field. For the investigated transition, the branch-

ing into other crystal field levels reduces this value to $P = 74(7)$.

The system is excited by faint laser pulses, and the resonant fluorescence is observed using single-photon detectors. The polarization of the excitation laser and the emitted photons are parallel to the D2 axis of the crystal. When scanning the excitation laser frequency and the cavity resonance in parallel, we observe many peaks that originate from single dopants, see Fig. 1c. Their emission is enhanced via the Purcell effect [3, 19] with enhancement factors up to $P = 70(12)$, depending on the dopant position in the cavity mode. Such P values, determined from lifetime measurements (not shown), are in excellent agreement with the expectation based on the resonator geometry. For $P \gg 1$, the erbium emission is almost fully channeled into the resonator, enabling high photon generation efficiency. In our setup, the probability that a photon leaves through the coupling mirror is 34(3) %, and 63(9) % of these photons are coupled into a single-mode optical fiber. The overall probability to

detect an emitted photon in our setup is further reduced to $\sim 2.4\%$ by the finite transmission and detector efficiency. Each of these values may be further improved in the future.

As a single dopant can only emit one photon at a time, on each peak we observe antibunching when measuring the photon temporal correlation function $g^2(\tau)$ [3] using a single detector. In Fig. 1d and e, we exemplary show the data for a randomly-chosen well-coupled dopant. For a perfect emitter and setup, $g^2(0) = 0$. In the depicted measurement, we observe a finite value of $0.73(4)$, which is explained by the dark counts of the detector (dashed line) and the excitation of a background that stems from other dopants which are weakly coupled to the resonator mode. After rescaling to eliminate the independently measured dark counts, we find $g^2(0) = 0.53(7)$. We then reduce the background contribution using excitation pulses of smaller spectral width, Fig. 1e. This leads to $g^2(0) = 0.34(8)$, testifying that we indeed observe a single emitter. With such narrowband pulses, the excitation probability is diminished if the laser frequency does not precisely match that of the emitter. The latter is not perfectly stable due to the fluctuating magnetic field caused by the nuclear spin bath in YSO, as characterized in detail below. This leads to the observation of bunching with a characteristic decay constant of $80(20)$ ms at large magnetic fields, here 6.8 T.

The change of the resonance frequency of the dopants happens on a timescale that is slow compared to their lifetime. Thus, using fast resonance frequency measurements [4], our setup can generate single photons with very narrow linewidth for application in extremely-dense wavelength division multiplexing. The limit of the current measurement is the pulse bandwidth of 0.28 MHz, while the ultimate limit is given by the radiative linewidth of 1.1 kHz FWHM (for the strongest coupled dopants), or by the emitter dephasing. To quantify the latter, we perform coherent spectroscopy.

COHERENT CONTROL OF INDIVIDUAL DOPANTS

To this end, we first establish coherent control over individual dopants by applying laser pulses of constant frequency on resonance with one of the peaks in the spectrum. When the intensity of the Gaussian excitation pulses of $1\text{ }\mu\text{s}$ duration (FWHM) is scanned, the fluorescence signal after the pulse shows coherent Rabi oscillations on all investigated dopants. In Fig. 2a, we again show exemplary data of a randomly-chosen emitter (blue triangle in Fig. 1c). We attribute the observed damping to a fluctuation of the pulse intensity which is caused by cavity resonance fluctuations by up to 6 MHz (FWHM) in the used closed-cycle cryocooler. Furthermore, also the background of weakly-coupled dopants contributes to the

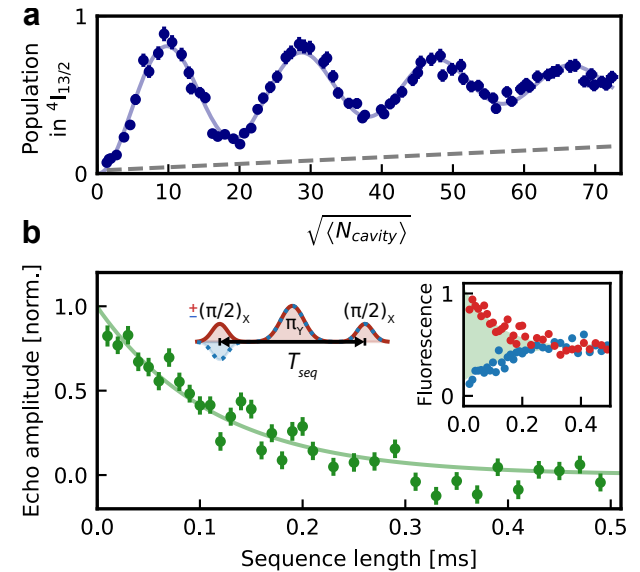


FIG. 2. **Optical coherence.** a) An excitation laser pulse of varying intra-cavity mean photon number $\langle N_{\text{cavity}} \rangle$ is applied to excite the fluorescence of a single dopant. The observation of Rabi oscillations proofs coherent control. The observed decay is well fit by a model (blue line) that includes cavity resonance fluctuations and the excitation of a background of weakly-coupled dopants (grey dashed line). b) Optical spin echo spectroscopy. To measure the optical coherence time, a laser pulse that performs a $\pi/2$ rotation is applied to the dopant. After a delay time of $T_{\text{seq}}/2$ (left inset), a π pulse cancels the effect of a static detuning between dopant and laser. Finally, another $\pi/2$ pulse is applied. The decay of the difference signal (green data and exponential fit) between measurements with unchanged (right inset, red) and inverted (blue) phase of the first pulse give an optical coherence time of $0.11(1)$ ms.

signal, leading to an increase that is linear to first order (grey dashed).

In addition, dephasing may contribute to the damping of Rabi oscillations. To study this, we perform optical spin echo measurements. First, a coherent superposition of the Z_{1-} ground and the Y_{1-} optically excited state is generated by a $\pm\pi/2$ -pulse. Then, a π -pulse cancels the effect of a static detuning between the emitter and the excitation pulse. Finally, another $\pi/2$ -pulse transfers the dopants to the ground or optically excited state, depending on the relative phase. Dephasing will reduce the contrast, i.e. the fluorescence signal difference between measurements with orthogonal phase of the two applied $\pi/2$ pulses. In Fig. 2b, we again show exemplary data from a randomly-chosen dopant (green triangle in Fig. 1c).

The dephasing times of all eight different emitters we measured (four each at 2 T and 6.8 T) are identical within errors, with an average of $T_2 = 0.115(7)$ ms. The corresponding homogeneous linewidth of 2.3 kHz improves by

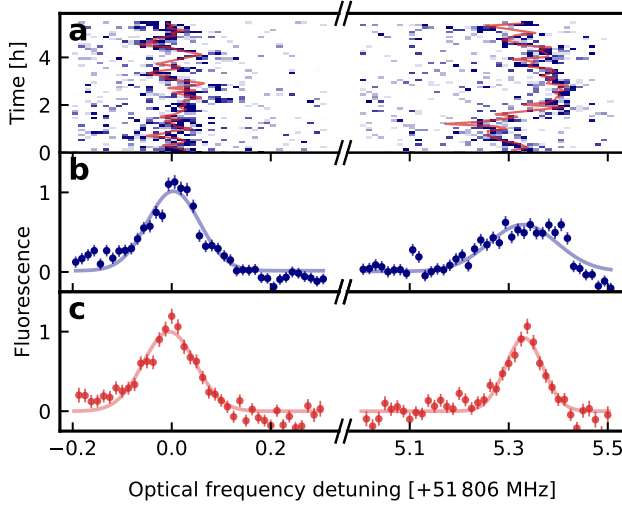


FIG. 3. Long-term spectral stability. Two ions, on resonance with the cavity, are optically excited in an alternating sequence with Gaussian pulses of 0.02 MHz FWHM spectral width. The fluorescence is measured as a function of the excitation laser detuning. a) When the results are averaged over 6 min intervals, the center of the line (red fit results) shows only small fluctuations. b) When averaging over the full 6 h measurement record, the Gaussian peaks of the fluorescence exhibit a FWHM of 0.14(1) MHz and 0.16(2) MHz. c) When applying feed-forward, i.e. shifting the laser frequency according to the fit center of the last interval to correct for slow frequency shifts, a further linewidth reduction to 0.10(1) MHz (red data and fit) is obtained, depending on the dopant.

a factor of 27 with respect to the narrowest single emitter linewidth reported so far [10]. Compared to ensemble measurements in the same setup [5], the coherence time is slightly reduced, which we attribute to a slightly increased sample temperature caused by the resonator stabilization laser. At lower temperature, lifetime-limited homogeneous linewidth can be achieved at the used resonator parameters [5].

LONG-TERM SPECTRAL STABILITY

After characterizing the short-term stability of the emitters, we now turn to long-term observations. In Fig. 3a, we again show exemplary data of two well-coupled dopants (orange triangles in Fig. 1c) that are detuned by 5.3 MHz and measured in an alternating sequence without cavity length changes. Only small fluctuations of the resonance frequency are observed between 6-minute measurement intervals. The spectral diffusion of both dopants is not correlated, meaning that its source is local to each emitter. We find a standard deviation of the fitted line centers (red) of 45 kHz. Averaging over time, Fig. 3b, we obtain Gaussian lines with 0.14(1) MHz and 0.16(2) MHz FWHM (blue).

None of the measured dopants exhibits any signatures of charge instability or blinking that is commonly observed with other solid state emitters [4, 22]. Over the course of several days, they all give similar temporal behavior to that shown in Fig. 3b. Averaging long-term measurements of six randomly-chosen dopants, we determine a spectral-diffusion linewidth of 0.152(8) MHz FWHM.

This value is much narrower than those observed previously with erbium [12, 13], other rare-earth dopants [9, 11], and any other single emitter [6, 7, 19]. It perfectly matches the width expected from the coupling to the fluctuating nuclear spin bath in YSO. Thus, a further reduction of the spectral diffusion is expected in hosts that contain less nuclear spins [24–27].

The absence of other, dominant sources of frequency instability enables the exploration of the dynamics of the "frozen core" of nuclear spins surrounding individual emitters [22]. As an example, we observe that some dopants (e.g. the right peak in Fig. 3) show occasional fast shifts of the center frequency exceeding 0.1 MHz. We attribute these shifts to flips of proximal ^{29}Si nuclear spins that have a natural isotopic abundance of $\sim 5\%$ and an expected lifetime that is consistent with the observed absence of such shifts over several hours.

Remarkably, the maximum expected ^{29}Si -Er coupling of 0.36 MHz can exceed the measured spectral-diffusion linewidth. Thus, our system may enable quantum network nodes with optically-interfaced nuclear-spin registers. In turn, undesired nuclear-spin induced shifts may be avoided in isotopically purified samples, or by applying a feed-forward operation. To implement the latter, we adapt the detuning of the excitation laser based on the center-frequency fit in the last measurement interval, achieving a further linewidth reduction below 0.10 MHz (in post-processing) for some dopants, as shown in Fig. 3c. Using this technique to further reduce the linewidth of all dopants would require faster resonance frequency measurements, ideally within the observed spectral diffusion timescale of 80(20) ms (see Fig. 1e). This may become feasible with further improvements of the experimental setup.

SUMMARY AND OUTLOOK

In summary, we have shown that the fluorescence of individual emitters in a solid can be enhanced without inducing significant dephasing or spectral diffusion by proximal interfaces. We can thus realize cavity-enhanced quantum network nodes with hundreds of emitters that are individually controlled via ultra-dense wavelength-division multiplexing. Compared to nanophotonic structures that typically feature GHz broad cavity linewidths [6, 8, 9, 11–14, 19], our resonator only enhances the emission within a narrow spectral range, which reduces un-

desired cross-talk and will enable direct spin-readout via selective fluorescence enhancement [3] at low magnetic fields. Still, using the built-in piezo to control the cavity resonance, one may switch between all optically resolved dopants on a sub-millisecond timescale [28], which may be further reduced by including electro-optic crystalline layers as host crystal [11] or additional tuning element.

The narrow homogeneous linewidth, slow spectral diffusion, and high photon generation efficiency of our setup will facilitate the entanglement of dopants over tens of kilometers of optical fiber via photon interference. To this end, long-enough ground-state coherence is achieved using hyperfine states of ^{167}Er [23] or host crystals with a low concentration of nuclear spins and erbium impurities [24–27] in order to avoid dephasing via spin-spin interactions [29].

The rates of local operations, currently limited by the 0.15 ms lifetime, may be further enhanced in silicon [24, 25] or other [27] host crystals, as well as in cavities with higher finesse and smaller mode waist [30]. Combining the two, one expects even Fourier-limited spectral diffusion linewidth, eliminating the need for fast resonance frequency measurements common in solid-state quantum network nodes [4]. Finally, our setup may enable the implementation of distributed quantum information processing with all-to-all connectivity in a rare-earth based quantum computer [16].

ACKNOWLEDGEMENTS

This project received funding from the European Research Council (ERC) under the European Union’s Horizon 2020 research and innovation programme (grant agreement No 757772), and from the Deutsche Forschungsgemeinschaft (DFG, German Research Foundation) under Germany’s Excellence Strategy - EXC-2111 - 390814868.

* andreas.reiserer@mpq.mpg.de

[1] S. Wehner, D. Elkouss, and R. Hanson, *Science* **362** (2018).

[2] C. Monroe and J. Kim, *Science* **339**, 1164 (2013).

[3] A. Reiserer and G. Rempe, *Rev. Mod. Phys.* **87**, 1379 (2015).

[4] M. Ruf, N. H. Wan, H. Choi, D. Englund, and R. Hanson, *Journal of Applied Physics* **130**, 070901 (2021).

[5] B. Merkel, A. Ulanowski, and A. Reiserer, *Phys. Rev. X* **10**, 041025 (2020).

[6] A. Faraon, P. E. Barclay, C. Santori, K.-M. C. Fu, and R. G. Beausoleil, *Nat. Photon.* **5**, 301 (2011).

[7] A. Sipahigil, R. E. Evans, D. D. Sukachev, M. J. Burek, J. Borregaard, M. K. Bhaskar, C. T. Nguyen, J. L. Pacheco, H. A. Atikian, C. Meuwly, R. M. Camacho, F. Jelezko, E. Bielejec, H. Park, M. Lončar, and M. D. Lukin, *Science* **354**, 847 (2016).

[8] D. Riedel, I. Söllner, B. J. Shields, S. Starosielec, P. Appel, E. Neu, P. Maletinsky, and R. J. Warburton, *Phys. Rev. X* **7**, 031040 (2017).

[9] T. Zhong, J. M. Kindem, J. G. Bartholomew, J. Rochman, I. Craicu, V. Verma, S. W. Nam, F. Marzili, M. D. Shaw, A. D. Beyer, and A. Faraon, *Phys. Rev. Lett.* **121**, 183603 (2018).

[10] J. M. Kindem, A. Ruskuc, J. G. Bartholomew, J. Rochman, Y. Q. Huan, and A. Faraon, *Nature* **580**, 201 (2020).

[11] K. Xia, F. Sardi, C. Sauerzapf, T. Kornher, H.-W. Becker, Z. Kis, L. Kovacs, R. Kolesov, and J. Wrachtrup, *arXiv:2104.00389* (2021).

[12] A. M. Dibos, M. Raha, C. M. Phenicie, and J. D. Thompson, *Phys. Rev. Lett.* **120**, 243601 (2018).

[13] S. Chen, M. Raha, C. M. Phenicie, S. Ourari, and J. D. Thompson, *Science* **370**, 592 (2020).

[14] D. Levonian, R. Riedinger, B. Machielse, E. Knall, M. Bhaskar, C. Knaut, R. Bekenstein, H. Park, M. Lončar, and M. Lukin, *arXiv:2108.10928* (2021).

[15] N. H. Nickerson, J. F. Fitzsimons, and S. C. Benjamin, *Phys. Rev. X* **4**, 041041 (2014).

[16] A. Kinos, D. Hunger, R. Kolesov, K. Mølmer, H. de Riedmatten, P. Goldner, A. Tallaire, L. Morvan, P. Berger, S. Welinski, K. Karrai, L. Rippe, S. Kröll, and A. Walther, *arXiv:2103.15743* (2021).

[17] H.-J. Briegel, W. Dür, J. I. Cirac, and P. Zoller, *Phys. Rev. Lett.* **81**, 5932 (1998).

[18] S. Sangtawesin, B. L. Dwyer, S. Srinivasan, J. J. Allred, L. V. H. Rodgers, K. De Greve, A. Stacey, N. Dontschuk, K. M. O’Donnell, D. Hu, D. A. Evans, C. Jaye, D. A. Fischer, M. L. Markham, D. J. Twitchen, H. Park, M. D. Lukin, and N. P. de Leon, *Phys. Rev. X* **9**, 031052 (2019).

[19] P. Lodahl, S. Mahmoodian, and S. Stobbe, *Rev. Mod. Phys.* **87**, 347 (2015).

[20] S. Zaske, A. Lenhard, C. A. Kefler, J. Kettler, C. Hepp, C. Arend, R. Albrecht, W.-M. Schulz, M. Jetter, P. Michler, and C. Becher, *Phys. Rev. Lett.* **109**, 147404 (2012).

[21] C. E. Bradley, J. Randall, M. H. Abobeih, R. C. Berrevoets, M. J. Degen, M. A. Bakker, M. Markham, D. J. Twitchen, and T. H. Taminiau, *Phys. Rev. X* **9**, 031045 (2019).

[22] G. Wolfowicz, F. J. Heremans, C. P. Anderson, S. Kanai, H. Seo, A. Gali, G. Galli, and D. D. Awschalom, *Nat. Rev. Mater.* **1**, 1 (2021).

[23] M. Rancić, M. P. Hedges, R. L. Ahlefeldt, and M. J. Sellars, *Nat. Phys.* **14**, 50 (2018).

[24] L. Weiss, A. Gritsch, B. Merkel, and A. Reiserer, *Optica* **8**, 40 (2021).

[25] A. Gritsch, L. Weiss, J. Früh, S. Rinner, and A. Reiserer, *arXiv:2108.05120* (2021).

[26] M. L. Dantec, M. Rancić, S. Lin, E. Billaud, V. Ranjan, D. Flanigan, S. Bertaina, T. Chanelière, P. Goldner, A. Erb, R. B. Liu, D. Estève, D. Vion, E. Flurin, and P. Bertet, *arXiv:2106.14974* (2021).

[27] P. Stevenson, C. M. Phenicie, I. Gray, S. P. Horvath, S. Welinski, A. M. Ferrenti, A. Ferrier, P. Goldner, S. Das, R. Ramesh, R. J. Cava, N. P. de Leon, and J. D. Thompson, *arXiv:2110.04876* (2021).

[28] B. Casabone, C. Deshmukh, S. Liu, D. Serrano, A. Ferrier, T. Hümmer, P. Goldner, D. Hunger, and H. de Riedmatten, *Nature Communications* **12**, 3570 (2021).

- [29] B. Merkel, P. Cova Fariña, and A. Reiserer, Phys. Rev. Lett. **127**, 030501 (2021).
- [30] G. Wachter, S. Kuhn, S. Minniberger, C. Salter, P. Asenbaum, J. Millen, M. Schneider, J. Schalko, U. Schmid, A. Felgner, D. Hüser, M. Arndt, and M. Trupke, Light Sci. Appl. **8**, 37 (2019).